Hybrid dansyl-triazine based mono and bidentate ligands for the selective sensing of fluoride anion through fluorescence enhancement

Ajay Jayaprakash[a],† Rakhi Mol K.M[a†], Mintu Porel[a,b]*

[a]*Department of Chemistry*

[b]*Environmental Sciences and Sustainable Engineering Centre*

Indian Institute of Technology Palakkad, Kerala 678557, India

*mintu@iitpkd.ac.in

† = Authors contributed equally

Contents

1. Materials and methods

All the chemicals were purchased from Sigma Aldrich, Alfa Aeser, Spectrochem, Merck and TCI and used without further purification. LC-MS experiments were carried out on a Shimadzu LC-MS-8045 with a Sprite TARGA C18 column (40 × 2.1 mm, 5 µm) monitoring at 210 nm and 254 nm with positive mode for mass detection. Solvents for LC-MS were water with 0.1% formic acid (solvent A) and acetonitrile with 0.1% formic acid (solvent B). Compounds were eluted at a flow rate of 0.5 mL/min with a gradient of 5% solvent B for 2 min, then linearly from 5% to 40% solvent B over 4 min, then from 40% to 60% for 10 min, and lastly, it was brought down to 5% solvent B in 2 min, and then the procedure proceeded till for 2 min before stopping. Before injecting the sample, the column was washed twice, once with 50% Solvent B and once with 95% Solvent B. ^{1}H NMR spectra were recorded on Bruker AV III 400 MHz. The data were analyzed by MestReNova (version 8.1.1). ^{1}H NMR shifts are reported in units of ppm relative to tetramethyl silane. The data are presented in the following order: chemical shift, peak multiplicity (s=singlet, d=doublet, t=triplet, m=multiplet) and proton number. Fluorescence was recorded on Perkin Elmer FL 6500. The absorption and emission spectra were plotted in OriginPro 8.5.1.

Theoretical Calculations: All calculations were carried out using the Gaussian 16 program package.[S1] Calculations were performed by the density functional theory (DFT) method with restricted B3LYP (Becke's three-parameter hybrid exchange functional and the Lee-Yang-Parr correlation functional)[S2] level, employing a basis set 6-31G (d).

Data Analysis: Each measurement was conducted three times independently, and the outcomes are presented as the average value along with the mean +/- standard deviation. Fluorescence lifetime data were analyzed using the Horiba EzTime platform. The standard deviation (σ) was interpreted as the noise level, and the limit of detection (LOD) was estimated via the 3σ approach, defined by the formula LOD = 3σ/k. The binding constant was derived using a Benesi-Hildebrand analysis.

2. Mass spectra

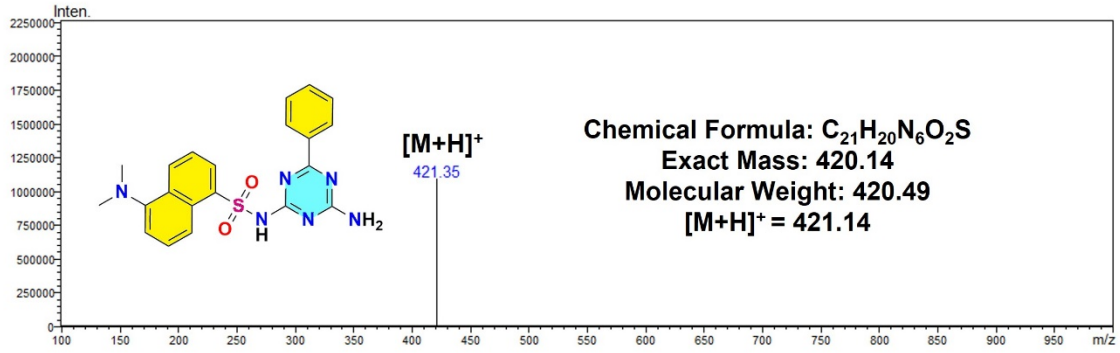

Figure S1. Mass spectrum of compound **DTM**.

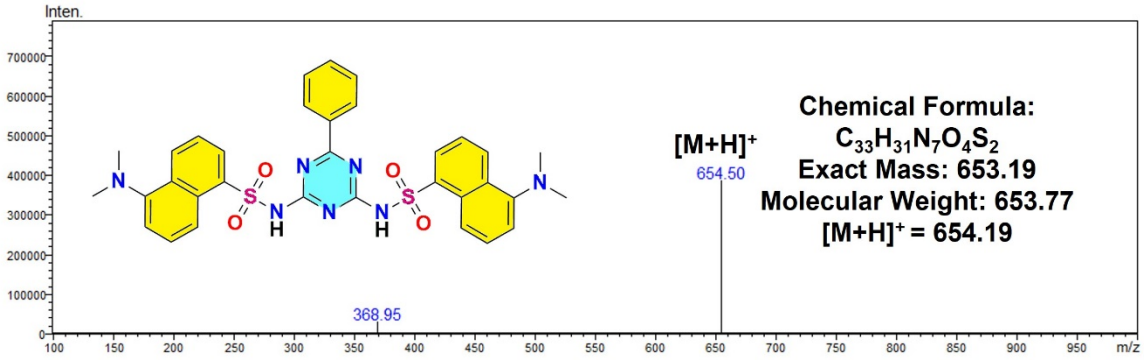

Figure S2. Mass spectrum of compound **DTD**.

3. NMR Spectra

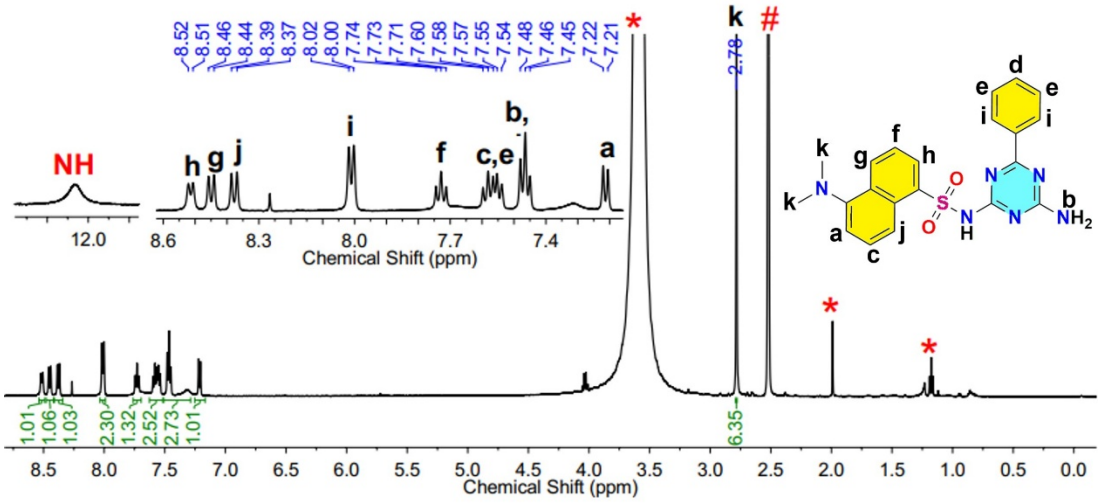

Figure S3. ^{1}H NMR spectrum of **DTM** recorded at 400 MHz in DMSO-d_6 at 298 K. Signals marked with (#) denotes DMSO peak and (*) represents residual solvent impurities and water respectively.

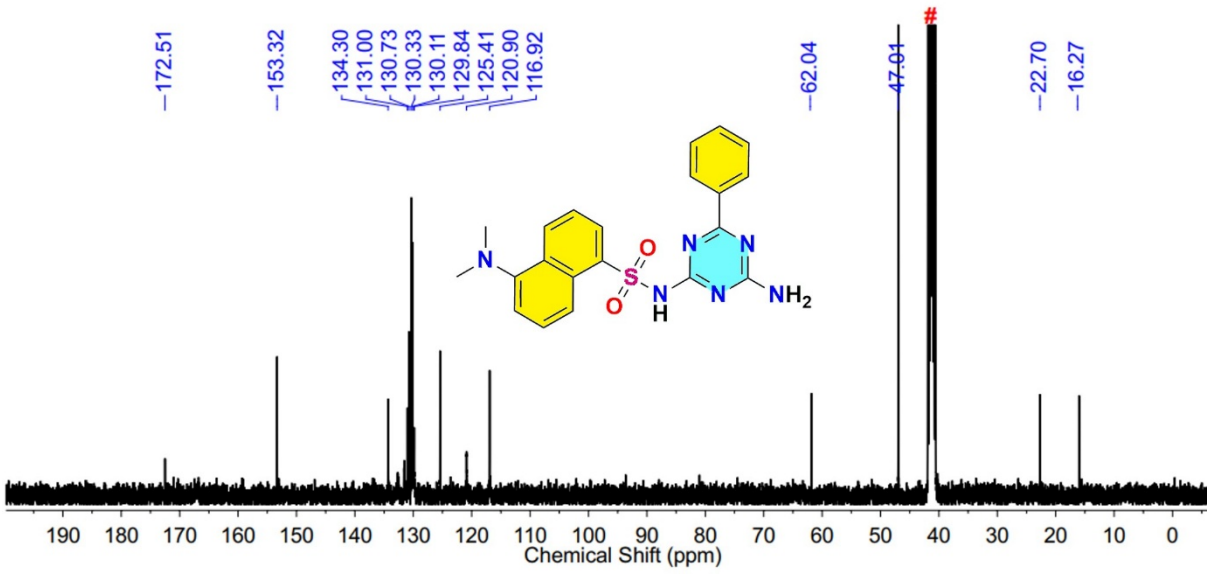

Figure S4. ^{13}C NMR spectrum of **DTM** recorded at 101 MHz in DMSO-d_6 at 298 K. Signal marked with (#) denotes residual carbon of DMSO-d_6.

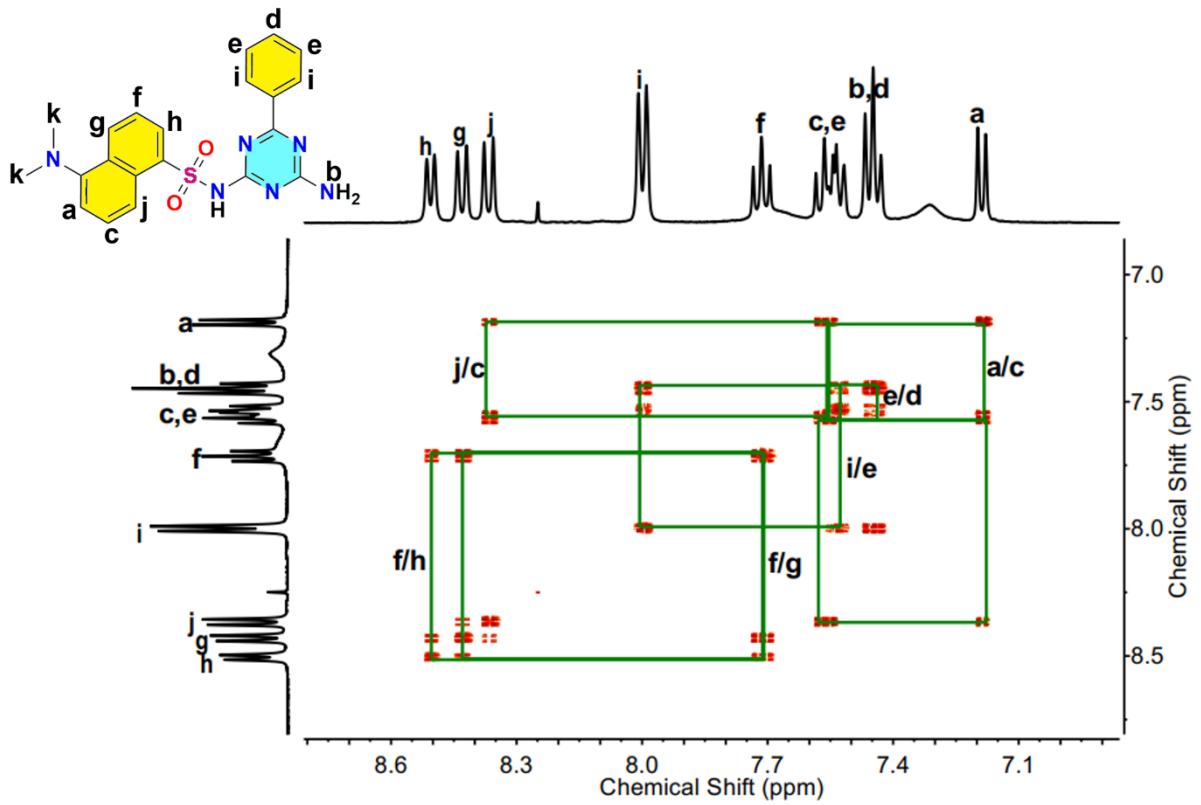

Figure S5. ^{1}H-^{1}H COSY spectrum of **DTM** recorded at 400 MHz in DMSO-d_6 at 298 K.

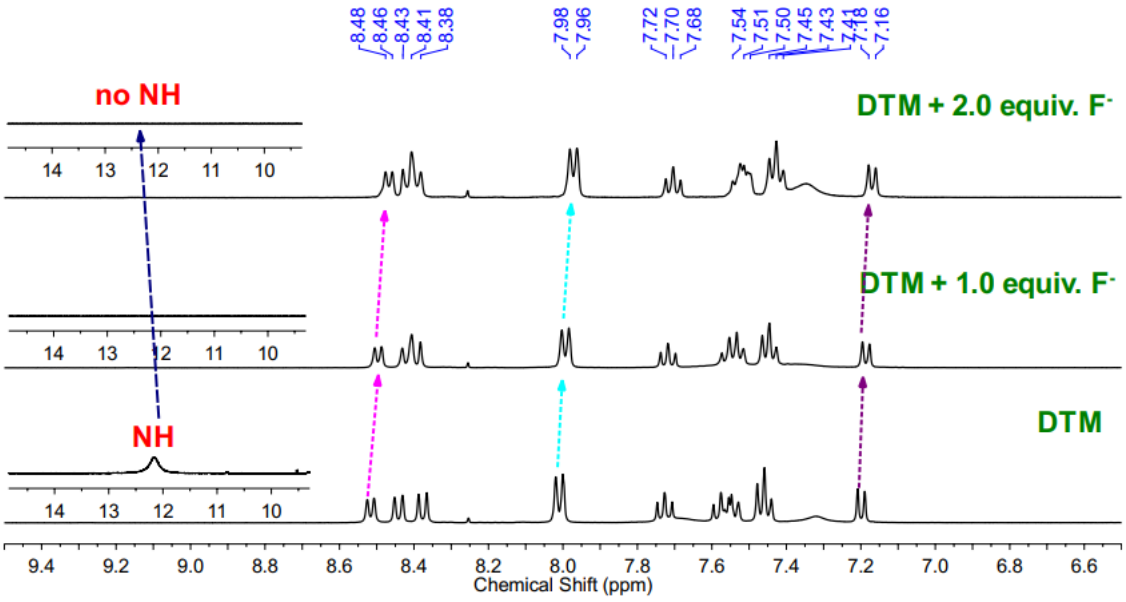

Figure S6. ^{1}H NMR spectral titration of **DTM** upon the addition of fluoride anion recorded at 400 MHz in DMSO-d_6 at 298 K.

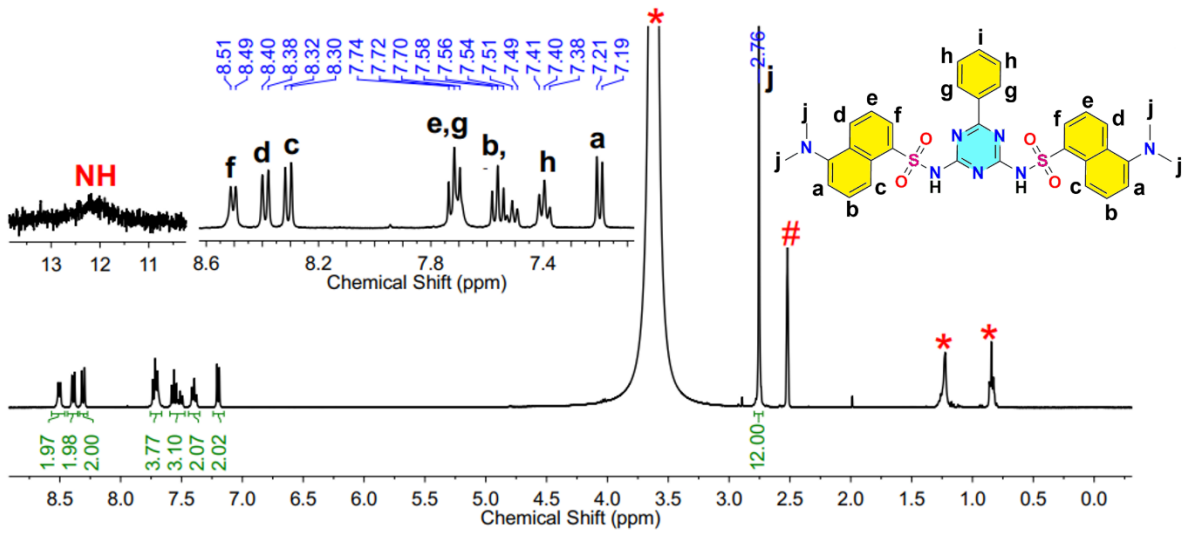

Figure S7. ^{1}H NMR spectrum of **DTD** recorded at 400 MHz in DMSO-d_6 at 298 K. Signals marked with (#) denotes DMSO peak (*) represent residual solvent impurities and water respectively.

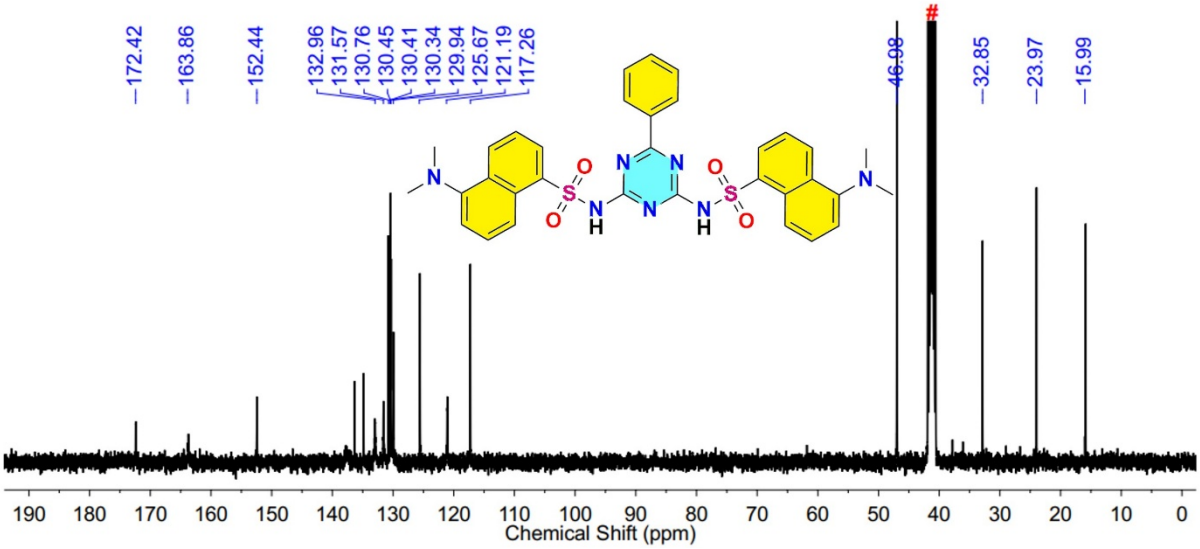

Figure S8. ^{13}C NMR spectrum of **DTD** recorded at 101 MHz in DMSO-d_6 at 298 K. Signal marked with (#) denotes residual carbon of DMSO-d_6.

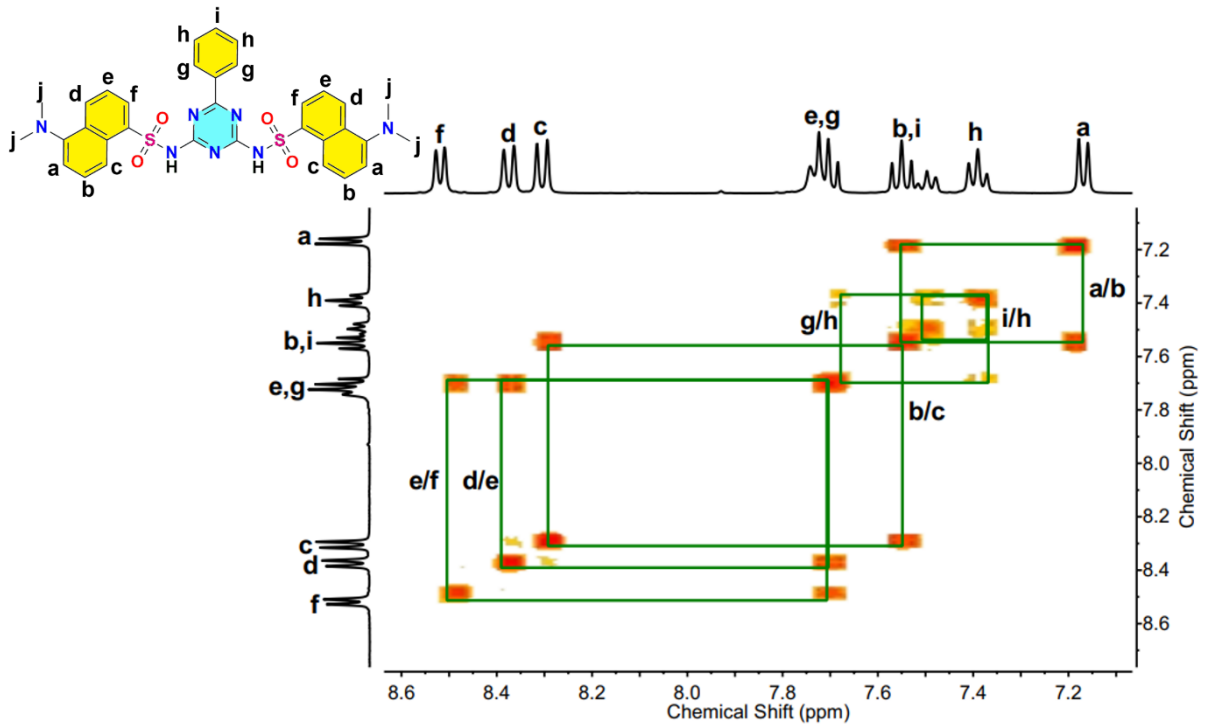

Figure S9. ^{1}H-^{1}H COSY spectrum of **DTD** recorded at 400 MHz in DMSO-d_6 at 298 K.

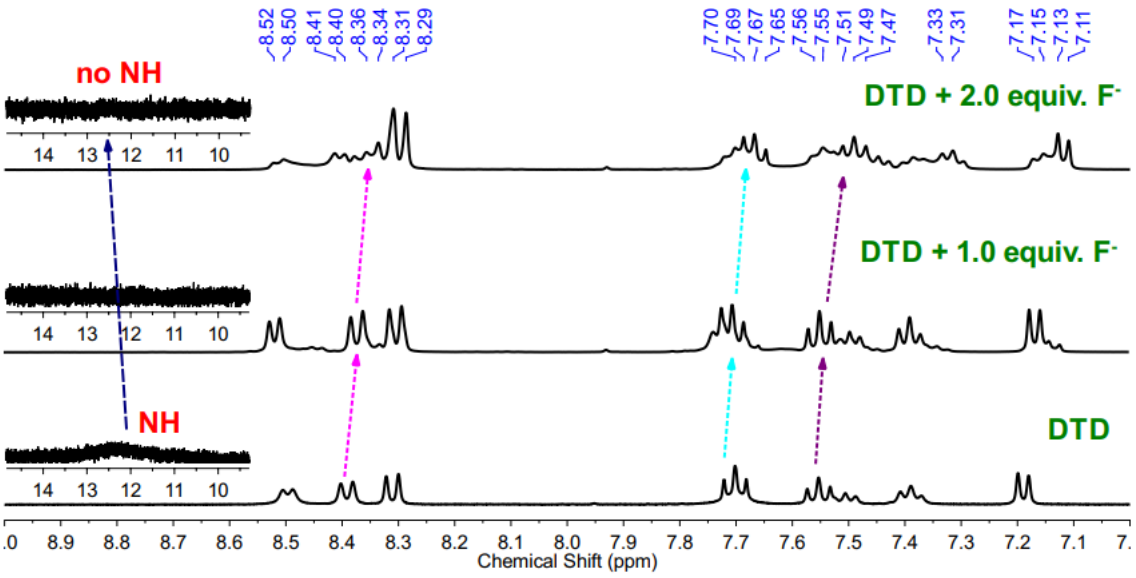

Figure S10. ^{1}H NMR spectral titration of **DTD** upon the addition of fluoride anion recorded at 400 MHz in DMSO-d_6 at 298 K.

4. Photophysical studies

4.1 UV- visible absorption and excitation-emission spectra

A 2 mM stock solution of **DTM** and **DTD** was prepared in DMSO. From these stock solutions, 20 µM aliquots were transferred to a cuvette containing 2 mL of DMSO, and their spectra were recorded. The absorption maxima were observed at 286 nm with a shoulder peak at 326 nm for **DTM**, while **DTD** exhibited absorption maxima at 288 nm and 327 nm. Upon excitation at 326 nm, the emission maxima were recorded at 481 nm for **DTM** and 462 nm for **DTD**.

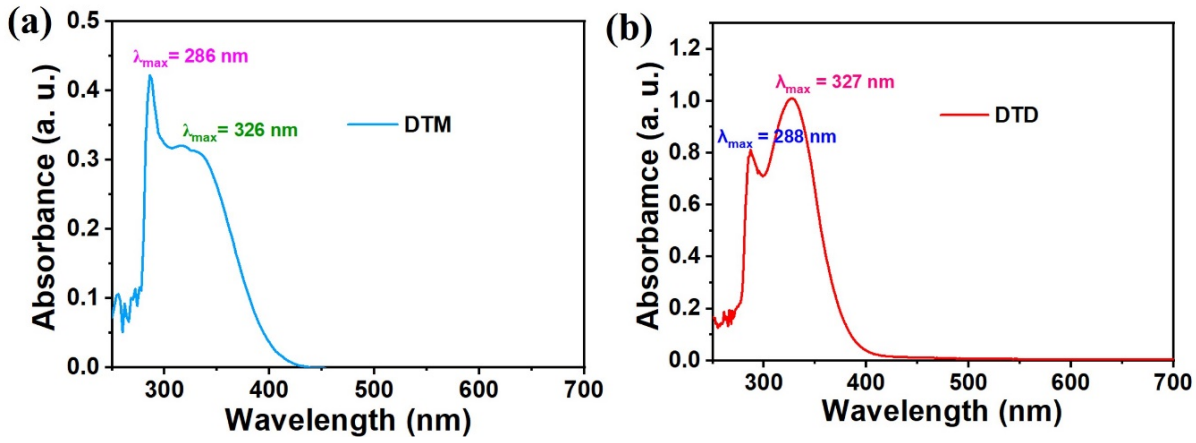

Figure S11. UV-visible absorption spectra of (a) **DTM** and (b) **DTD**

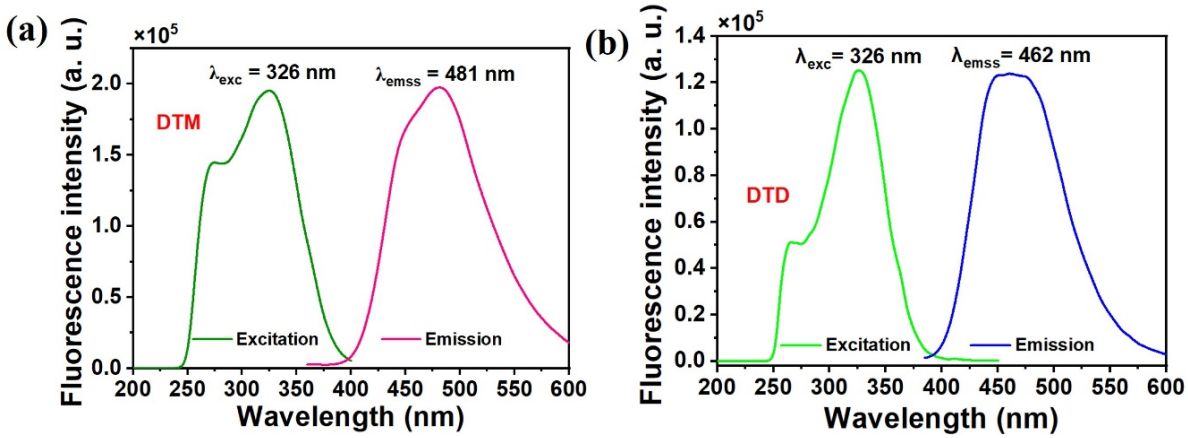

Figure S12. Excitation and emission spectra of (a) **DTM** and (b) **DTD**

4.2 Quantum yield calculation

The quantum yield of the **DTM** and **DTD** were calculated by taking quinine sulphate as reference. The quantum yield was calculated using the following equation:

$$Q_S = Q_R \frac{I_S}{I_R} \frac{A_R}{A_S} \frac{\eta_S^2}{\eta_R^2}$$

Q_S and Q_R denote the quantum yield of the sample and reference, respectively. I_S and I_R represent the integrated areas under the emission spectra for the sample and reference, while A_S and A_R correspond to the absorbance of the sample and reference. η represents the refractive index of the medium. The reference compound, quinine sulphate, had a quantum yield of 0.54. The quantum yields for **DTM** and **DTD** were determined to be 0.40 and 0.22, respectively.

5. Detection of fluoride anion

5.1 Selectivity studies

A 2 mM stock solution of **DTM** and **DTD** was prepared in DMSO. Subsequently, 10 μM sensor solutions were prepared by diluting the stock in 2 mL of DMSO and transferred into a cuvette for recording the fluorescence spectra. Separately, 5 mM stock solutions of tetrabutylammonium salts of various anions, including fluoride (F^-), chloride (Cl^-), bromide (Br^-), iodide (I^-), tetrafluoroborate (BF_4^-), hexafluorophosphate (PF_6^-), thiocyanate (SCN^-), hydrogen sulphate (HSO_4^-), and dihydrogen phosphate ($H_2PO_4^-$), were also prepared in DMSO. To each 10 μM sensor solution, 100 μM of the respective 5 mM anion stock was added, and the fluorescence spectra were recorded.

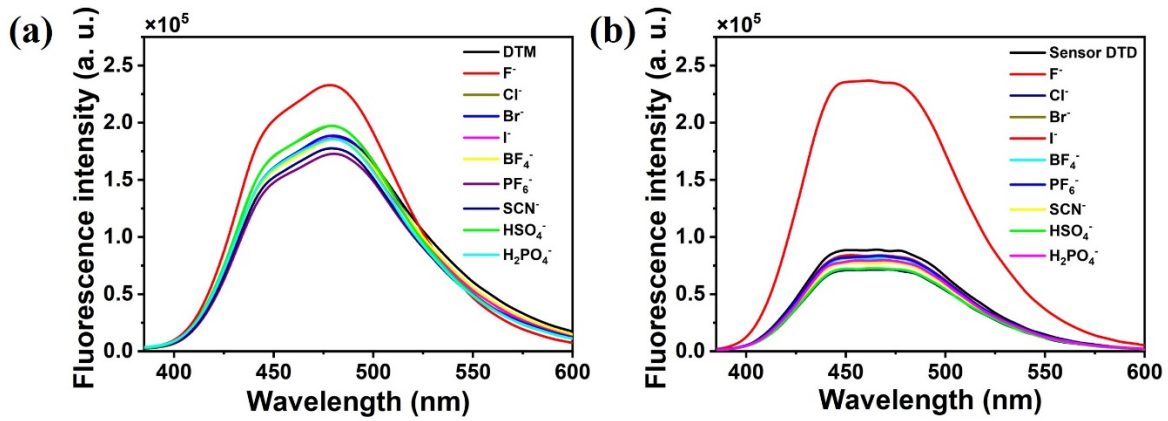

Figure S13. Selectivity of fluoride (F^-) with respect to other anions (a) **DTM** and (b) **DTD** when excited at 326 nm.

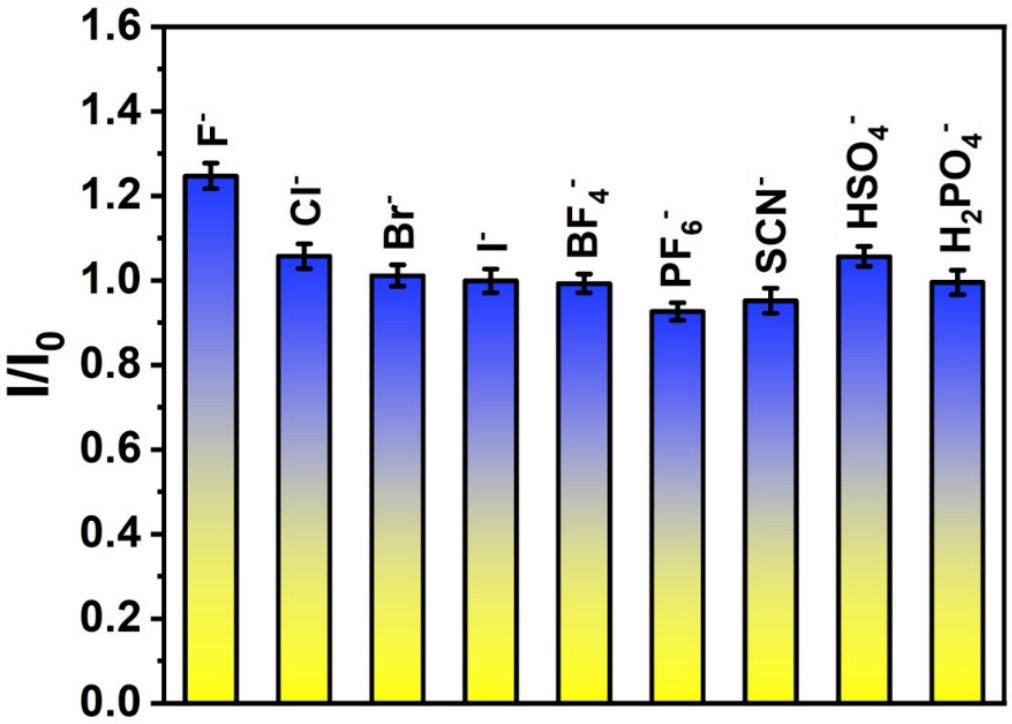

Figure S14. Selectivity bar diagram of fluoride (F^-) with respect to other anions for **DTM;** I and I_0 are the fluorescence intensity of the sensor in presence and absence of analytes respectively.

5.2 Fluorescence titration of DTM and DTD with fluoride

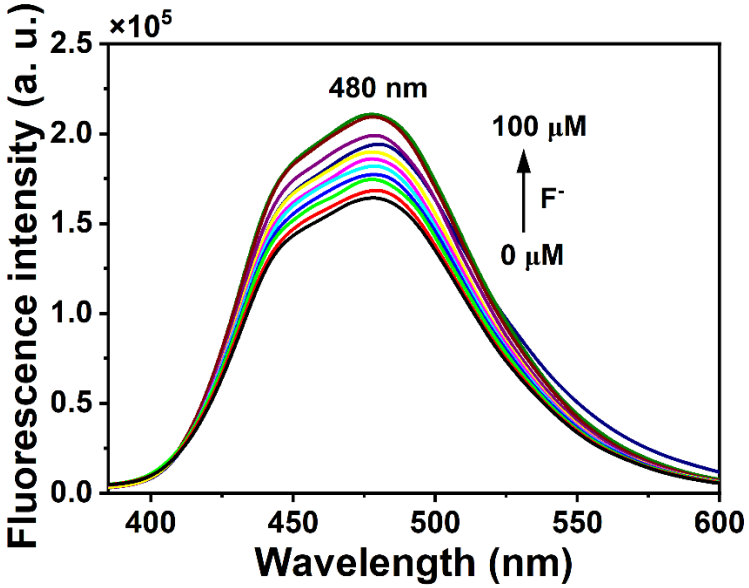

Figure S15. The fluorescence spectra of the sensor **DTM** (10 µM) after the addition of fluoride (0-100 µM) in DMSO at 25 ^{0}C when excited at 326 nm.

5.3 Limit of detection (LOD)

The limit of detection of **DTM** and **DTD** were determined using the **3σ/K** method, where **σ** represents the standard deviation and **K** denotes the slope of the fluorescence intensity of the sensor versus the concentration of fluoride anion (F^-).

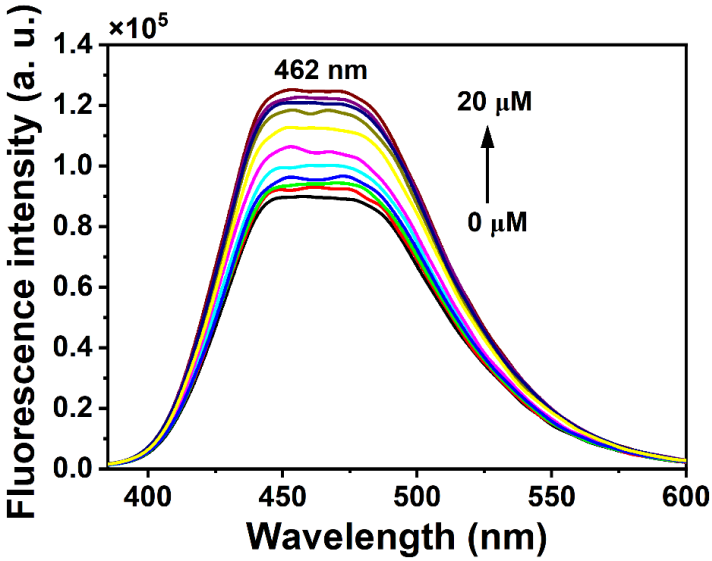

Figure S16. The fluorescence spectra of the sensor **DTD** (10 μM) after the addition of fluoride (0-20 μM) in DMSO at 25 ^{0}C when excited at 326 nm.

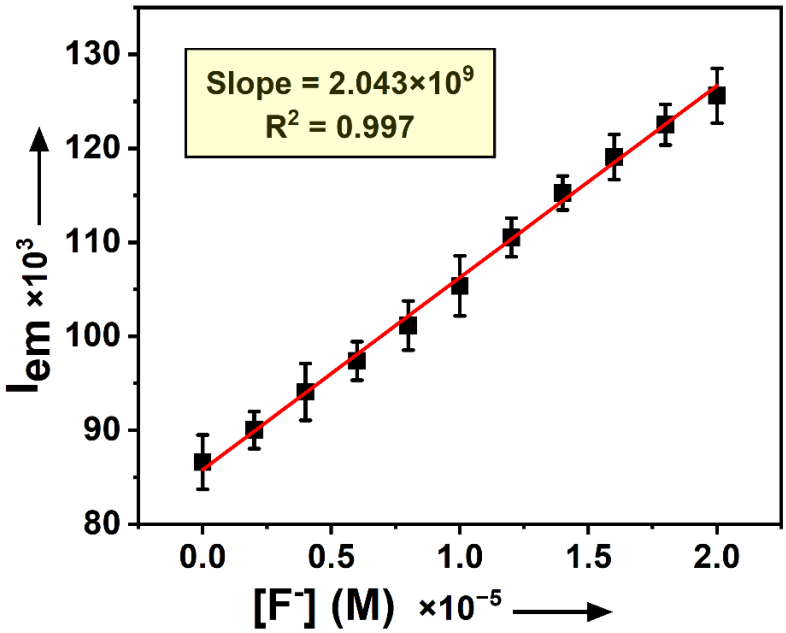

Figure S17. Fluorescence intensity vs concentration of fluoride anion curve of **DTD** (10 μM in DMSO) at 25 °C upon adding 0-20 μM of fluoride (excitation wavelength = 326 nm).

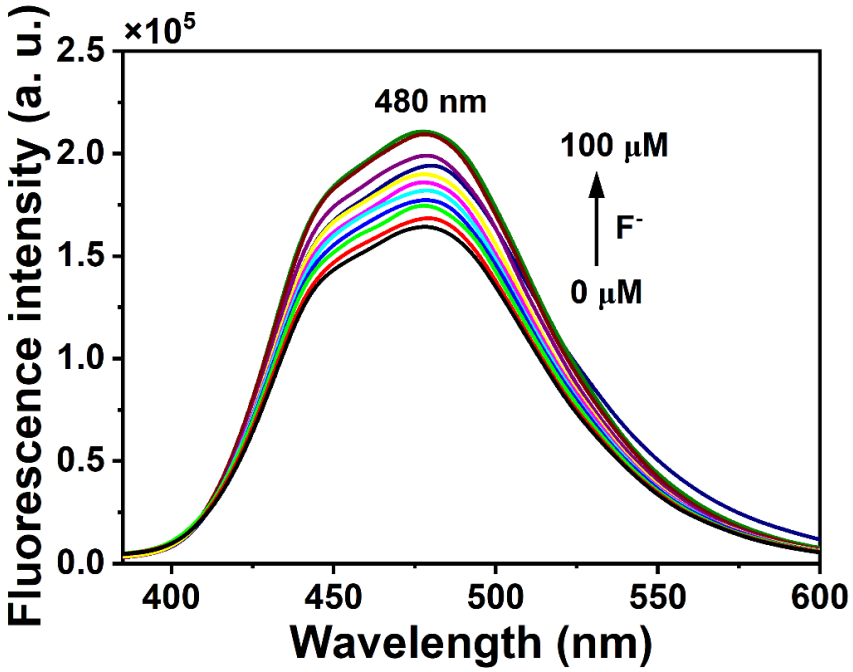

Figure S18. The fluorescence spectra of the sensor **DTM** (10 μM) after the addition of fluoride (0-100 μM) in DMSO at 25 ^{0}C when excited at 326 nm.

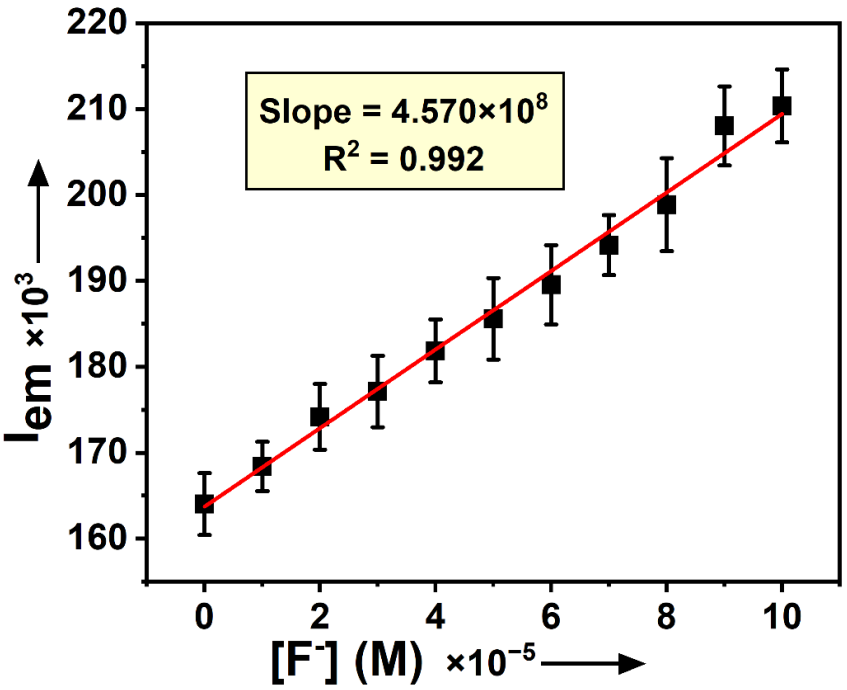

Figure S19. Fluorescence intensity vs concentration of fluoride anion curve of **DTM** (10 μM in DMSO) at 25 °C upon adding 0-20 μM of fluoride (excitation wavelength = 326 nm).

5.4 Benesi-Hildebrand plot- Determination of association constant K_a

The binding constant of **DTM** and **DTD** with the fluoride anion were determined using emission intensity data and analyzed according to the Benesi-Hildebrand equation.

$$\frac{1}{\Delta I} = \frac{1}{\Delta I_{max}} + \left(\frac{1}{K_a[F]}\right)\left(\frac{1}{\Delta I_{max}}\right)$$

Where $\Delta I = I - I_{min}$ and $\Delta I_{max} = I_{max} - I_{min}$, I_{min}, I, and I_{max} represent the emission intensities of the sensor in the absence of fluoride anions, at an intermediate fluoride concentration, and at full saturation, respectively. Here, K_a denotes the binding constant, and [F] represents the fluoride concentration. The value of K_a is determined from the slope and intercept of the plot of $[1 / (I – I_{min})]$ versus 1/[F].

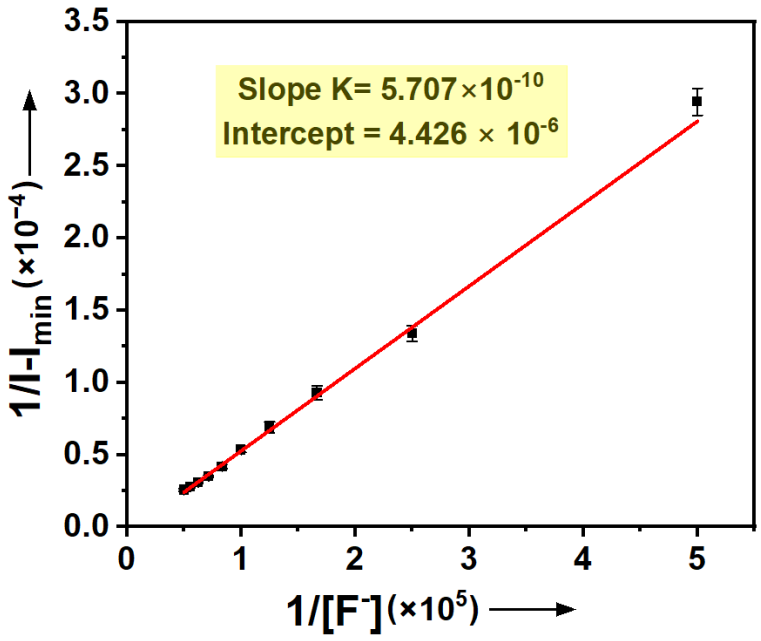

Figure S20. Benesi-Hildebrand plot for **DTD**

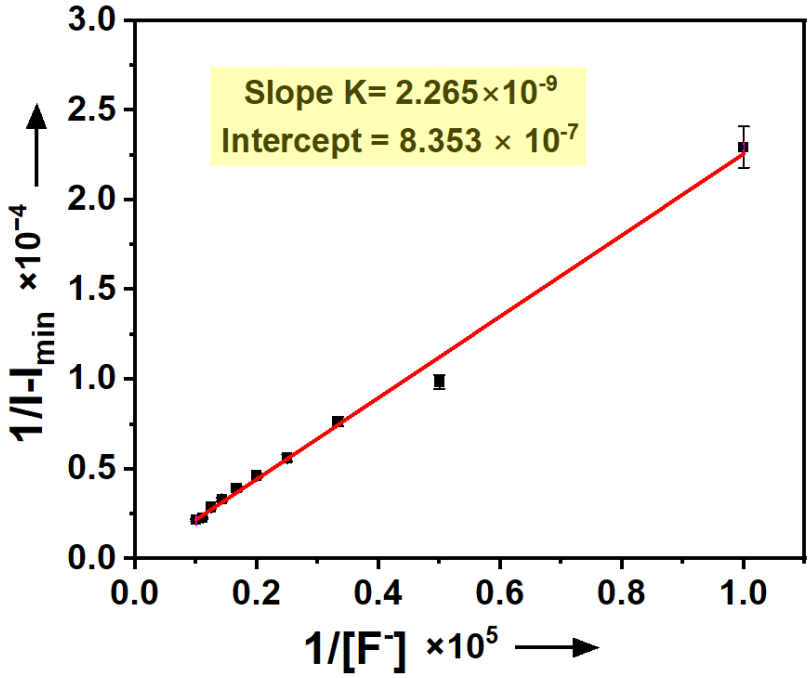

Figure S21. Benesi-Hildebrand plot for **DTM**

5.5 Competivity studies

A 10 µM solution of **DTM** and **DTD** in DMSO were taken in a cuvette and the fluorescence spectra were recorded. To that solution, 100 µM of other anions were added individually and recorded the spectra. Finally, a similar concentration of fluoride was added to the same solution and the emission spectra was recorded.

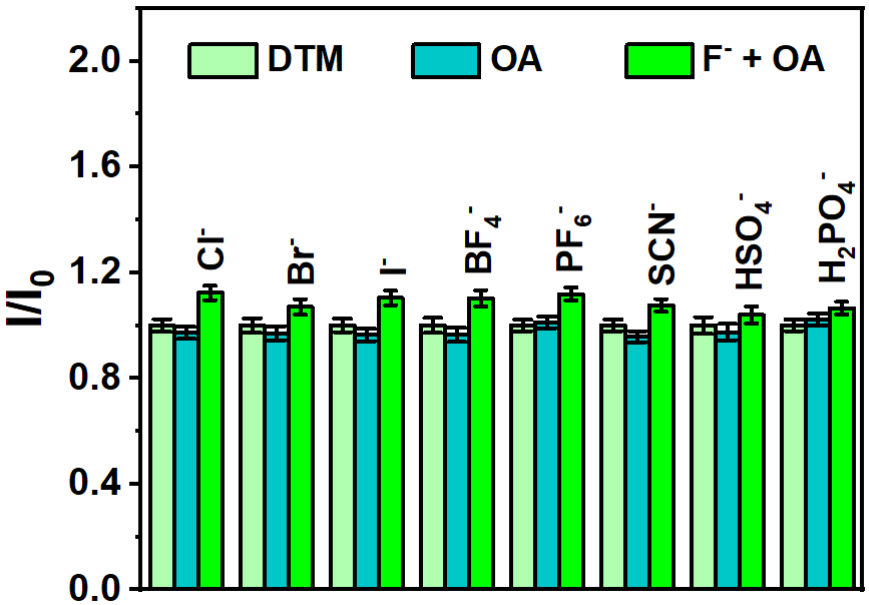

Figure S22. Competivity bar diagram of fluoride (F^-) with respect to other anions for **DTM**

5.6 Lifetime measurements

A 2 mM stock solution of **DTM** and **DTD** was prepared in DMSO and 10 μM of the sensor solution in DMSO were taken for the TCSPC analysis. Then 50 μM fluoride was added separately and the fluorescence decay profile was recorded.

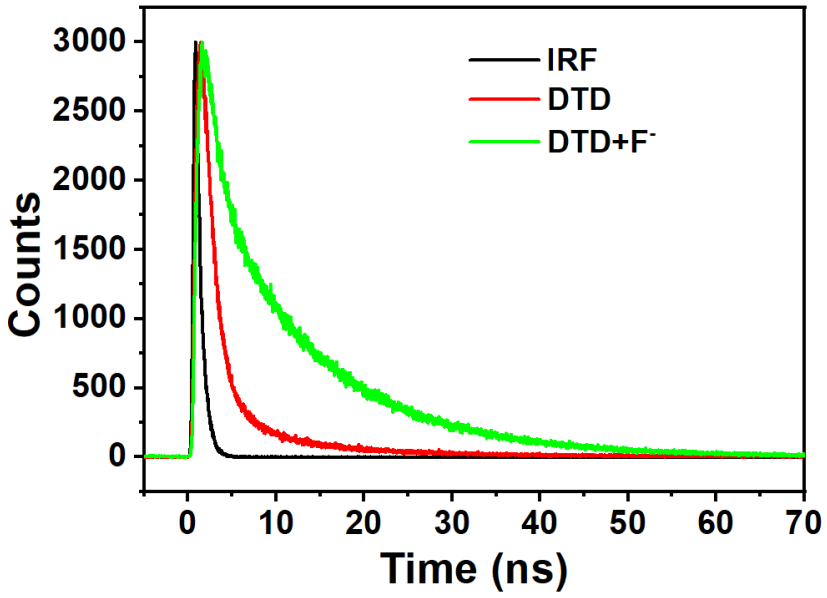

Figure S23. The fluorescence decay profiles for **DTD + F^-** (τ = 1.65 ns for **DTD**, τ = 6.23 ns for **DTD+F^-**).

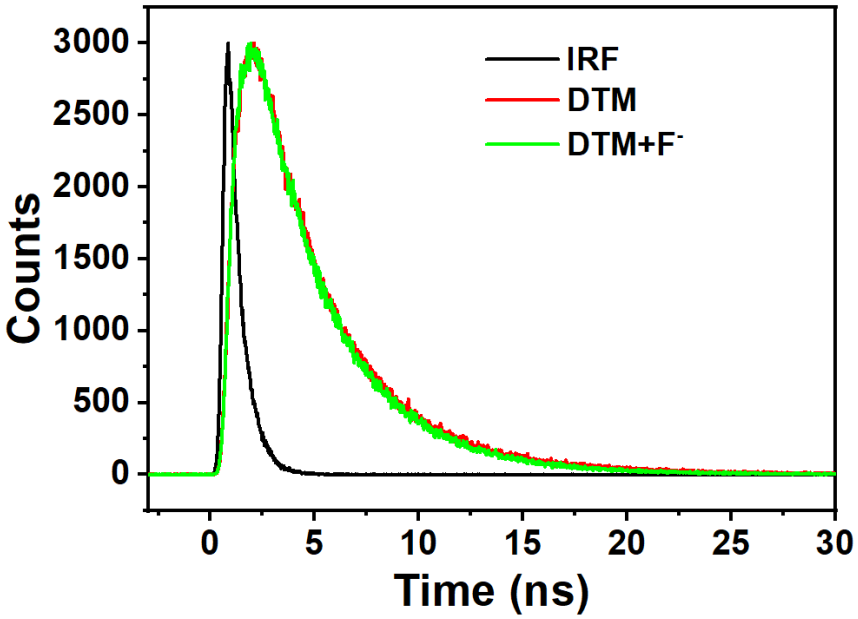

Figure S24. The fluorescence decay profiles for **DTM + F^-** (τ = 3.56 ns for **DTM** as well as **DTM+ F^-**)

5.8 Detection of fluoride anion in water

A 2 mM stock solution of DTM and DTD was prepared in DMSO. From this stock, a 10 µM sensor solution was prepared in 2 mL of water. To this solution, 100 µM anion solutions were added, and the spectra were recorded.

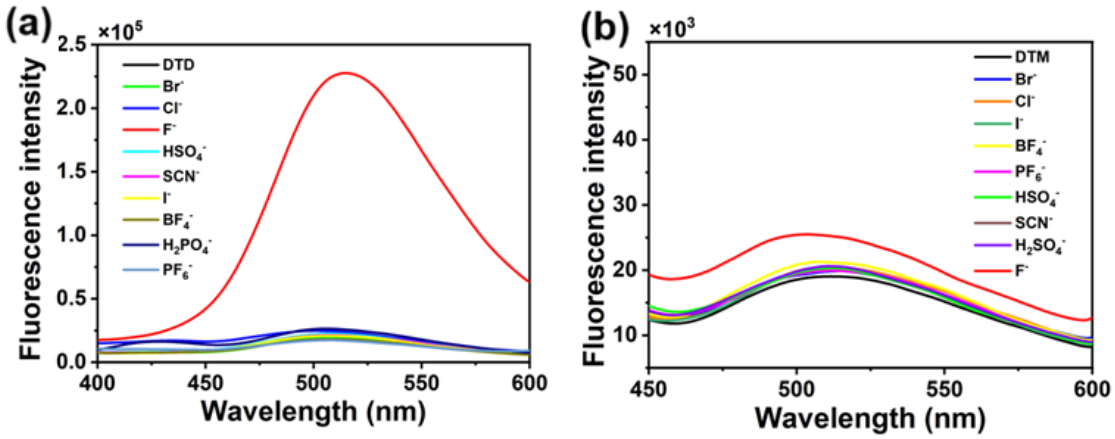

Figure S25. Selectivity of fluoride (F^-) with respect to other anions in water (a) **DTD** and (b) **DTM** when excited at 326 nm.

5.8 Real sample analysis

A 2 mM stock solution of **DTD** was prepared in DMSO. For spectral analysis, 10 µM of the sensor solution was transferred into a cuvette and diluted to 2 mL with distilled water. Then emission spectra were recorded. Subsequently, 50 µM of fluoride anion solution was spiked into the same cuvette, and the spectra were recorded again. This procedure was repeated using tap water, lake water, and pond water as real samples instead of distilled water.

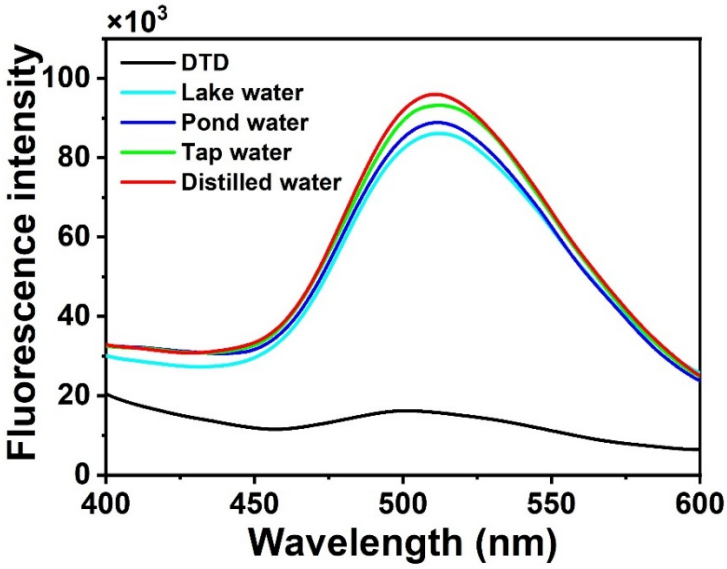

Figure S26. Detection of fluoride (F^-) in real water samples.

5.9 Paper strip-based detection of fluoride

Using **DTD**, we developed a cost-effective and portable paper strip for fluoride detection. Small strips of Whatman filter paper were prepared, with **DTD** solution individually coated at the centre. After drying, the strips were placed in a UV chamber, where a non-fluorescent spot was observed. Upon adding fluoride anion solution to the sensor spot, the fluorescence intensity was enhanced, indicating fluoride presence.

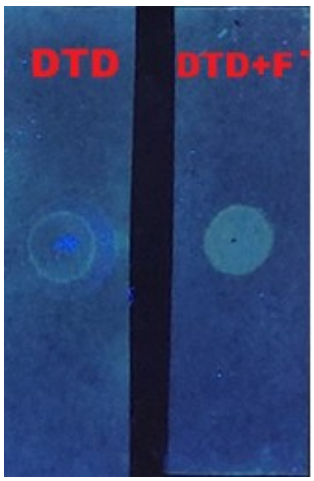

Figure S27. Photograph of detection of fluoride by **DTD** coated paper-strip under UV lamp.

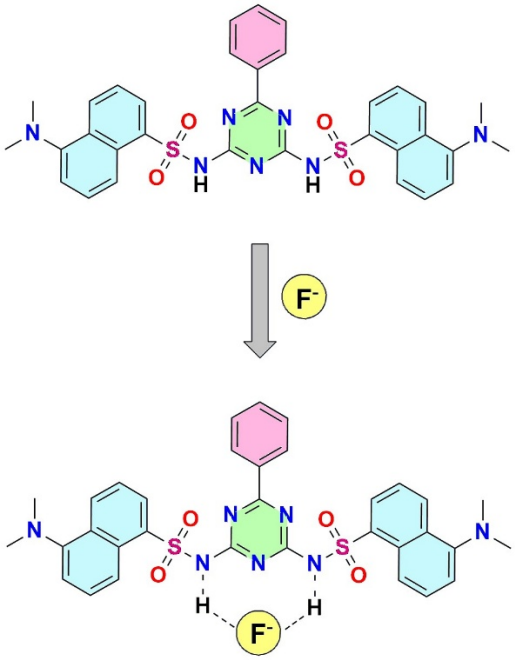

Figure S28. Mechanism for the sensing of fluoride anion.

Table S1: Various known fluoride sensors reported in the literature

Sensor	LOD	Journal
Transition Metal based fluoride sensors		
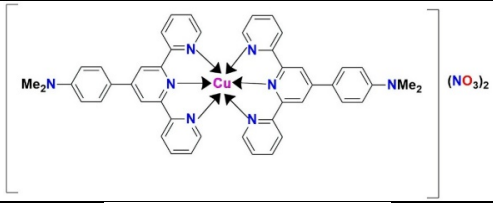	5.07 µM	P. K. Kar and co-workers, *Photochem. Photobiol. Sci.*, 2018, **17**, 815-821.
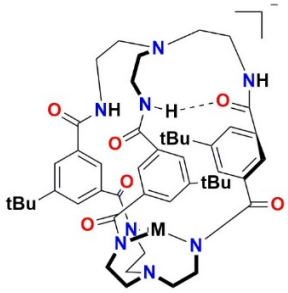	2-5 ppm	C. C. Cummins and co-workers, *Inorg. Chem.* 2017, **56**, 7615-7619.
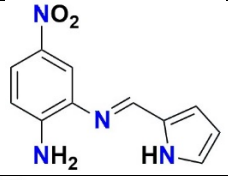	0.12 µM	S. P. Mahanta.and co-workers, *New J. Chem.*, 2018, **42**, 3758-3764.
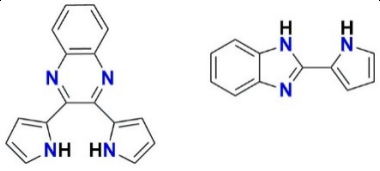	0.15 ppm	S. P. Mahanta.and co-workers, *New J. Chem.*,2019, **43**, 3447-3453

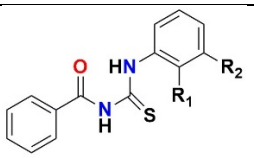 C1: $R_1 = R_2 = H$ C2: $R_1 = OH, R_2 = H$ C3: $R_1 = H, R_2 = OH$	1.07 ppm	S. P. Mahanta and co-workers, *Dalton Trans.*, 2021,**50**, 15287-15295
Silicon based fluoride sensors		
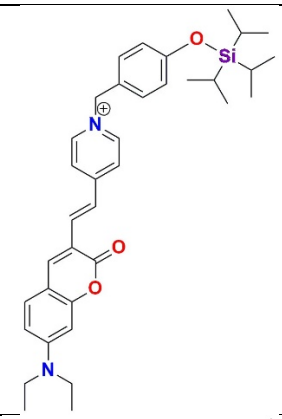	1.2×10^{-8} M	Y. Chen and co-workers, Sens. Actuators, B, 2018, **258**, 544–549
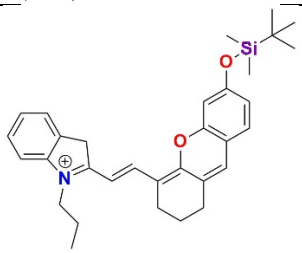	0.2 µM	X. Yang and co-workers, J. Agric. Food Chem., 2018, **66**, 11486–11491.
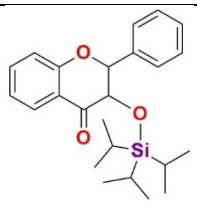	0.68 µM	Y. Fang and co-workers, Dyes Pigm., 2019, **166**, 473–479.
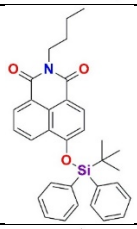	------	X. Zhang and co-workers, Sensors, 2015, 15, 1611–1622.
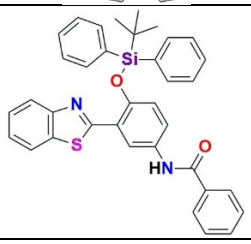	100 ppb	G. Yang and co-workers , Angew. Chem., Int. Ed., 2010, **49**, 4915–4918
Imidazole based fluoride sensors		
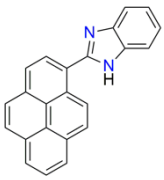	1.63×10^{-5} M	D. Das and co-workers , New J. Chem., 2018, **42**, 9200–9208

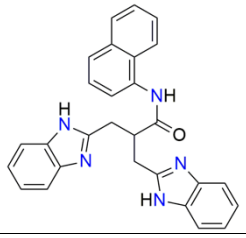	0.875 ppb	G. Das and co-workers, New J. Chem., 2019, **43**, 16497–16505
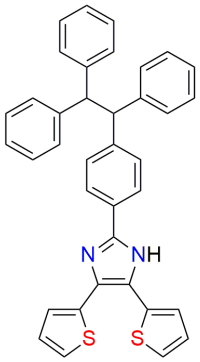	1.37×10^{-7} M	S. K. Bhargava and co-workers, Chemosensors, 2021, **9**, 285
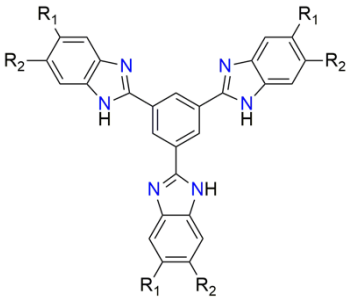	0.284 M -0.563 M	Z. Y. Wang and co-workers, Sens. Actuators, B, 2016, 237, 865–875
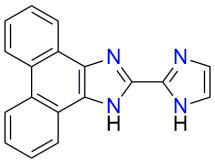	------	R. V. Solomon and co-workers, J. Photochem. Photobiol., A, 2022, 423, 113612
OH based fluoride sensors		
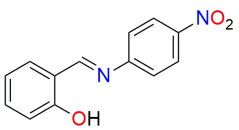	------	S. Velmathi and co-workers, Spectrochim. Acta - Part A Mol. Biomol. Spectrosc. 2010, **75**, 1146–1151
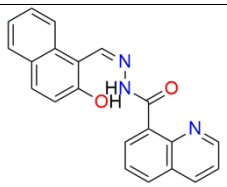	8.28 µM	L. Ren and co-workers Inorganica Chim. Acta. 2018, **476**, 7–11
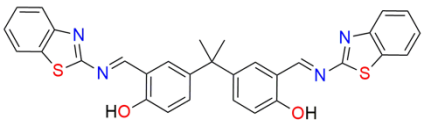	9.13 µM (UV-Vis) 3.47 µM (Fluorescence)	O. Kocyigit and co-workers, Sensors Actuators, B Chem. 2015, **221**, 900–905.
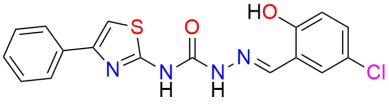	0.25 µM	F. Rahaman and co-workers, Spectrochimica Acta Part A: Molecular and Biomolecular

		Spectroscopy 2022, **264**, 120301
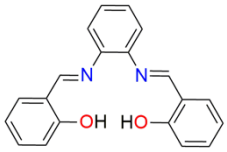	------	Sandeep Kumar Dey a and Christoph Janiak, RSC Adv., 2020, 10, 14689–14693
NH based fluoride sensors (Urea and Thiourea)		
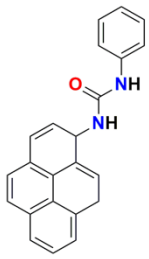	------	Sha Ding and co-workers, Spectrochimica Acta Part A: Molecular and Biomolecular Spectroscopy 2021, **246**, 118992
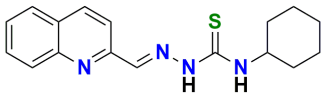	1–18 × 10^{-7} M	Sabeel M. Basheer and co-workers, Scientific Reports, 2025, **15**, 1859
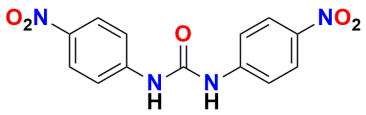	------	Boiocchi and co-workers, *J. AM. CHEM. SOC*., 2004, **126**, 16513
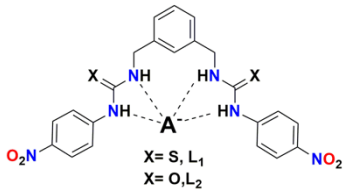	------	Md. Alamgir Hossain and co-workers, Frontiers in Chemistry, 2021, **8**, 1-7
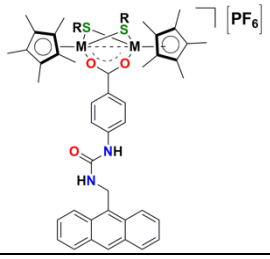	9 µM	Jingping Qu and co-workers, Dalton Trans., 2016, **45**, 6839–6846
NH based sensor without urea entity and metals		
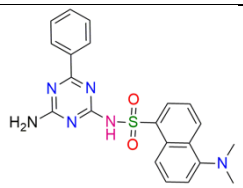	1.31 µM	This work
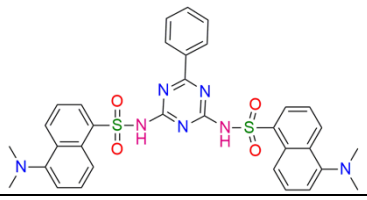	294 nM	This work

6. DFT Calculations

Cartesian coordinates for DTM, DTM+F$^-$, DTD and DTD+F$^-$

DTM: B3LYP/6-31G(d) level: (found 0 imaginary frequencies)

Optimization energy Eopt = -1689.393090 Hartree

Center Number	Atomic Number	Atomic Type	Coordinates (Angstroms) X	Y	Z
1	6	0	0.779521	0.655948	1.397508
2	7	0	0.226127	1.244760	0.321089
3	6	0	-0.917785	0.692691	-0.100511
4	7	0	-1.515300	-0.366799	0.476816
5	6	0	-0.856790	-0.864613	1.524870
6	7	0	0.290646	-0.418023	2.043269
7	6	0	-1.576885	1.291303	-1.285532
8	6	0	-1.027463	2.425031	-1.904870
9	6	0	-1.648006	2.986538	-3.017731
10	6	0	-2.822116	2.423209	-3.525117
11	6	0	-3.372516	1.294466	-2.913483
12	6	0	-2.755458	0.729783	-1.799699
13	7	0	-1.421476	-1.938600	2.196187
14	16	0	-2.521349	-3.076830	1.538889
15	7	0	1.921866	1.202410	1.881591
16	8	0	-2.112431	-3.444078	0.185887
17	8	0	-2.562843	-4.090929	2.595598
18	6	0	-4.087170	-2.175262	1.548028
19	6	0	-4.415380	-1.648555	2.782243
20	6	0	-5.624588	-0.953769	2.961209
21	6	0	-6.512844	-0.847838	1.915245
22	6	0	-6.238663	-1.429994	0.652720
23	6	0	-4.972461	-2.081308	0.424126
24	6	0	-7.199568	-1.339623	-0.417243

25	6	0	-6.851125	-1.792104	-1.675332
26	6	0	-5.590481	-2.385294	-1.901957
27	6	0	-4.678885	-2.555477	-0.886398
28	7	0	-8.469440	-0.761249	-0.133801
29	6	0	-9.381136	-1.633392	0.614597
30	6	0	-9.148250	-0.114710	-1.248749
31	1	0	-0.116215	2.851306	-1.500619
32	1	0	-1.216534	3.864671	-3.490813
33	1	0	-3.305006	2.862732	-4.394252
34	1	0	-4.284537	0.850174	-3.302974
35	1	0	-3.174260	-0.147557	-1.321103
36	1	0	-0.845980	-2.350389	2.924974
37	1	0	2.394038	1.891698	1.316792
38	1	0	-3.725673	-1.749712	3.612983
39	1	0	-5.845529	-0.499004	3.922138
40	1	0	-7.434319	-0.288397	2.029221
41	1	0	-7.557315	-1.720930	-2.495876
42	1	0	-5.347627	-2.742372	-2.899350
43	1	0	-3.731786	-3.036977	-1.079495
44	1	0	-10.214126	-1.038016	1.005333
45	1	0	-9. 796975	-2.439111	-0.015882
46	1	0	-8.861580	-2.095001	1.456453
47	1	0	-9.973816	0.487894	-0.853998
48	1	0	-8.454211	0.549643	-1.770505
49	1	0	-9.575855	-0.823283	-1.981290
50	1	0	2.445253	0.686717	2.572460

DTM+F^-: B3LYP/6-31G(d) level: (found 0 imaginary frequencies)

Optimization energy Eopt = - -1789.145331 Hartree

Center	**Atomic**	**Atomic**	**Coordinates (Angstroms)**		
Number	**Number**	**Type**	**X**	**Y**	**Z**

1	6	0	-4.367224	0.060440	-0.790950
2	7	0	-3.812114	1.276476	-0.660088
3	6	0	-2.564527	1.288851	-0.162050
4	7	0	-1.843252	0.197685	0.173512
5	6	0	-2.477967	-0.962785	0.006844
6	7	0	-3.736417	-1.060176	-0.425104
7	6	0	-1.919313	2.609316	0.016007
8	6	0	-2.613147	3.786667	-0.308351
9	6	0	-2.004716	5.027413	-0.140825
10	6	0	-0.698617	5.107540	0.350168
11	6	0	-0.003799	3.939850	0.674020
12	6	0	-0.608244	2.696121	0.509875
13	7	0	-1.874149	-2.168925	0.230124
14	16	0	-0.482807	-2.487401	1.175627
15	7	0	-5.610801	-0.078625	-1.281416
16	8	0	-0.565535	-1.729757	2.419920
17	8	0	-0.458362	-3.949177	1.189711
18	6	0	0.869459	-1.907688	0.126529
19	6	0	0.951042	-2.581069	-1.077887
20	6	0	1.956457	-2.258793	-2.006092
21	6	0	2.899601	-1.307756	-1.688315
22	6	0	2.886141	-0.643409	-0.436771
23	6	0	1.819191	-0.900049	0.498994
24	6	0	3.909916	0.316543	-0.108838
25	6	0	3.797751	1.048101	1.057784
26	6	0	2.724105	0.823519	1.946294
27	6	0	1.770062	-0.136037	1.699878
28	7	0	4.989845	0.486390	-1.020588
29	6	0	5.985548	-0.590848	-0.992338
30	6	0	5.625575	1.797143	-1.032075
31	1	0	-3.625545	3.710995	-0.688490
32	1	0	-2.548653	5.933678	-0.392819

33	1	0	-0.225173	6.077325	0.480041
34	1	0	1.012167	3.995273	1.055205
35	1	0	-0.075557	1.786222	0.759948
36	1	0	-2.490779	-2.966782	0.047520
37	1	0	-6.095961	0.723259	-1.651557
38	1	0	0.225869	-3.351682	-1.316489
39	1	0	1.978525	-2.759204	-2.969405
40	1	0	3.662607	-1.027589	-2.405558
41	1	0	4.553327	1.782540	1.316028
42	1	0	2.669345	1.403626	2.863857
43	1	0	0.975995	-0.310149	2.410573
44	1	0	6.625111	-0.517286	-1.879144
45	1	0	6.628459	-0.538819	-0.096057
46	1	0	5.493475	-1.565234	-1.001039
47	1	0	6.257245	1.871822	-1.924162
48	1	0	4.862873	2.578846	-1.082268
49	1	0	6.268618	1.987827	-0.153712
50	1	0	-5.939188	-1.019356	-1.453158
51	9	0	-4.301360	-2.934846	-0.841431

DTD: B3LYP/6-31G(d) level: (found 0 imaginary frequencies)

Optimization energy Eopt = -2756.602152 Hartree

Center	**Atomic**	**Atomic**	**Coordinates (Angstroms)**		
Number	**Number**	**Type**	**X**	**Y**	**Z**
1	6	0	-0.942232	-2.097622	-0.128077
2	7	0	-0.969069	-0.766314	-0.087892
3	6	0	0.214739	-0.186137	0.172796
4	7	0	1.351027	-0.861510	0.415376
5	6	0	1.229790	-2.189605	0.379679
6	7	0	0.117211	-2.883528	0.100170
7	6	0	0.264954	1.290822	0.193076

8	6	0	-0.860434	2.039114	-0.189326
9	6	0	-0.810066	3.430496	-0.175451
10	6	0	0.358107	4.087065	0.221410
11	6	0	1.479768	3.346220	0.602642
12	6	0	1.437175	1.954631	0.587828
13	7	0	2.358510	-2.954442	0.599637
14	16	0	3.778710	-2.457739	1.430258
15	7	0	-2.130747	-2.766892	-0.375039
16	16	0	-3.450638	-2.165282	-1.294337
17	8	0	-2.955314	-1.296891	-2.359321
18	8	0	-4.179954	-3.393534	-1.621498
19	6	0	-4.395202	-1.192038	-0.110210
20	8	0	3.407535	-1.709709	2.627759
21	8	0	4.507090	-3.722773	1.544762
22	6	0	4.610242	-1.415230	0.213386
23	6	0	4.777666	-2.022302	-1.016426
24	6	0	5.438696	-1.348401	-2.058245
25	6	0	5.972176	-0.099743	-1.833194
26	6	0	5.877988	0.526062	-0.565370
27	6	0	5.140556	-0.113304	0.496184
28	6	0	6.479279	1.816581	-0.342061
29	6	0	6.255293	2.465078	0.857309
30	6	0	5.494579	1.850792	1.875070
31	6	0	4.969353	0.588758	1.723380
32	6	0	-5.444608	-0.340102	-0.589797
33	6	0	-6.203285	0.379082	0.397841
34	6	0	-5.944090	0.157065	1.774936
35	6	0	-4.942060	-0.690238	2.186764
36	6	0	-4.150295	-1.363903	1.235020
37	6	0	-5.793077	-0.196735	-1.961440
38	6	0	-6.846922	0.608016	-2.323432
39	6	0	-7.567408	1.353532	-1.365729

40	6	0	-7.247171	1.277692	-0.022972
41	7	0	-7.928080	2.032241	0.973234
42	7	0	7.265047	2.382129	-1.385249
43	6	0	8.596040	1.784253	-1.538407
44	6	0	7.327031	3.836877	-1.431928
45	6	0	-7.160938	3.158806	1.515138
46	6	0	-9.298479	2.420043	0.667239
47	1	0	-1.757470	1.516420	-0.501916
48	1	0	-1.681839	4.004318	-0.477809
49	1	0	0.394248	5.173495	0.231620
50	1	0	2.390889	3.851538	0.911123
51	1	0	2.302305	1.371637	0.881863
52	1	0	2.214854	-3.958498	0.652224
53	1	0	-2.056372	-3.776771	-0.458561
54	1	0	4.374533	-3.014074	-1.189673
55	1	0	5.515110	-1.814456	-3.035848
56	1	0	6.454640	0.445817	-2.636052
57	1	0	6.689435	3.442657	1.038394
58	1	0	5.346922	2.378346	2.813783
59	1	0	4.416000	0.129623	2.529090
60	1	0	-6.581867	0.648274	2.500855
61	1	0	-4.761851	-0.857613	3.244356
62	1	0	-3.358639	-2.026419	1.561920
63	1	0	-5.231251	-0.718814	-2.724519
64	1	0	-7.114532	0.698208	-3.372652
65	1	0	-8.362520	2.011550	-1.699816
66	1	0	9.021774	2.088245	-2.501302
67	1	0	9.288069	2.100556	-0.738128
68	1	0	8.529381	0.694829	-1.518628
69	1	0	7.745258	4.138282	-2.398663
70	1	0	6.320067	4.253886	-1.346092
71	1	0	7.961226	4.281002	-0.643308

72	1	0	-7.640073	3.516014	2.433697
73	1	0	-6.142975	2.846404	1.755692
74	1	0	-7.102742	4.002238	0.804491
75	1	0	-9.777216	2.769699	1.588630
76	1	0	-9.375145	3.234366	-0.076040
77	1	0	-9.854537	1.555298	0.295467

DTD+F^-: B3LYP/6-31G(d) level: (found 0 imaginary frequencies)

Optimization energy Eopt = -2856.405415 Hartree

Center Number	**Atomic Number**	**Atomic Type**	**Coordinates (Angstroms) X**	**Y**	**Z**
1	6	0	0.767761	-1.907182	-0.304159
2	7	0	1.033942	-1.067665	0.693412
3	6	0	-0.029990	-0.713329	1.442140
4	7	0	-1.303293	-1.091210	1.212658
5	6	0	-1.468262	-1.920856	0.182185
6	7	0	-0.452651	-2.374021	-0.558908
7	6	0	0.225943	0.173629	2.595117
8	6	0	1.544615	0.504982	2.948281
9	6	0	1.785794	1.333706	4.040196
10	6	0	0.718726	1.841047	4.785671
11	6	0	-0.594495	1.514539	4.437867
12	6	0	-0.842899	0.683054	3.349867
13	7	0	-2.692885	-2.362641	-0.229310
14	16	0	-4.160129	-2.382536	0.662681
15	7	0	1.737963	-2.326822	-1.178676
16	16	0	3.428692	-2.390785	-0.870707
17	8	0	3.637368	-2.735833	0.532155
18	8	0	3.907022	-3.268935	-1.938060
19	6	0	3.970760	-0.699504	-1.173072
20	8	0	-5.028107	-3.183124	-0.199848
21	8	0	-3.878867	-2.785720	2.035886

22	6	0	-4.684733	-0.666117	0.674218
23	6	0	-4.727072	-0.068445	1.916512
24	6	0	-5.118329	1.280050	2.031605
25	6	0	-5.484133	1.987859	0.909550
26	6	0	-5.499439	1.385776	-0.375236
27	6	0	-5.059250	0.024689	-0.523583
28	6	0	-5.912433	2.130524	-1.536865
29	6	0	-5.784258	1.550748	-2.785691
30	6	0	-5.319460	0.225518	-2.922654
31	6	0	-4.990747	-0.537032	-1.827138
32	6	0	5.240629	-0.260692	-0.670613
33	6	0	5.640219	1.082107	-0.998281
34	6	0	4.825852	1.864255	-1.856461
35	6	0	3.629545	1.387432	-2.338981
36	6	0	3.191022	0.096405	-1.985393
37	6	0	6.127317	-1.073914	0.088388
38	6	0	7.346001	-0.577892	0.485291
39	6	0	7.725973	0.752927	0.210463
40	6	0	6.886998	1.596970	-0.492855
41	7	0	7.216374	2.952981	-0.769275
42	7	0	-6.414069	3.448372	-1.349274
43	6	0	-7.777562	3.511115	-0.809176
44	6	0	-6.242085	4.370388	-2.464613
45	6	0	6.471357	3.936658	0.024513
46	6	0	8.636238	3.276484	-0.821489
47	1	0	2.362471	0.097802	2.365297
48	1	0	2.807084	1.581381	4.313094
49	1	0	0.909943	2.487154	5.637673
50	1	0	-1.424196	1.907283	5.017867
51	1	0	-1.855587	0.420086	3.068395
52	1	0	-2.639417	-3.010609	-1.019444
53	1	0	1.413674	-2.993568	-1.878012

54	1	0	-4.436880	-0.641546	2.788916
55	1	0	-5.112764	1.758104	3.005837
56	1	0	-5.743739	3.037443	0.982303
57	1	0	-6.073978	2.101148	-3.673629
58	1	0	-5.252189	-0.209224	-3.915513
59	1	0	-4.693454	-1.567584	-1.959525
60	1	0	5.189240	2.840782	-2.153656
61	1	0	3.023187	1.992607	-3.004999
62	1	0	2.246830	-0.274375	-2.364353
63	1	0	5.845551	-2.082701	0.356207
64	1	0	8.021721	-1.213169	1.050142
65	1	0	8.677340	1.116603	0.581972
66	1	0	-7.982753	4.527425	-0.457157
67	1	0	-8.536301	3.247554	-1.565434
68	1	0	-7.887433	2.826493	0.032765
69	1	0	-6.441312	5.387485	-2.112239
70	1	0	-5.212698	4.327295	-2.827821
71	1	0	-6.922163	4.175468	-3.312387
72	1	0	6.590058	4.929469	-0.421834
73	1	0	5.408691	3.690792	0.038419
74	1	0	6.825753	3.983163	1.068473
75	1	0	8.753666	4.266626	-1.273364
76	1	0	9.122987	3.305688	0.169276
77	1	0	9.160823	2.549060	-1.445135
78	9	0	-0.957309	-3.463383	-2.151421

7. Supporting References

[S1] Gaussian 16, Revision C.01, Frisch MJ, Trucks GW, Schlegel HB, Scuseria GE, Robb MA, Cheeseman JR, Scalmani G, Barone V, Petersson GA, NakatsujiH, Li X, Caricato M, Marenich AV, Bloino J, Janesko BG, Gomperts R, Mennucci B, Hratchian HP, Ortiz JV, Izmaylov AF, Sonnenberg JL, Williams-Young D, Ding F, Lipparini F, Egidi F, Goings J, Peng B, Petrone A, Henderson T, Ranasinghe D, Zakrzewski VG, Gao J, Rega N, Zheng G, Liang

W, Hada M, Ehara M, Toyota K, Fukuda R, Hasegawa J, Ishida M, Nakajima T, Honda Y, Kitao O, Nakai H, Vreven T, Throssell K, Montgomery JA Jr, Peralta JE, Ogliaro F, Bearpark M, Heyd JJ, Brothers EN, Kudin KN, Staroverov VN, Keith T, Kobayashi R, Normand J, Raghavachari K, Rendell A, Burant JC, Iyengar SS, Tomasi J, Cossi M, Millam J M, Klene M, Adamo C, Cammi R, Ochterski JW, Martin RL, Morokuma K, Farkas O, Foresman JB, Fox DJ. Gaussian, Inc., Wallingford CT, 2016.

[S2] (a) A. D. Becke, *J. Chem. Phys.,* **1993**, *98*, 1372; (b) C. Lee, W. Yang and R. G. Parr, *Phys. Rev. B*, **1988**, *37*, 785.